Physics Letters B 815 (2021) 136101

Contents lists available at ScienceDirect

Physics Letters B

www.elsevier.com/locate/physletb

Production of neutron-rich $N = 126$ nuclei in multinucleon transfer reactions: Comparison between ^{136}Xe + ^{198}Pt and ^{238}U + ^{198}Pt reactions

K. Zhao [a,b,*], Z. Liu [c,d,*], F.S. Zhang [e,f,g], N. Wang [b,h]

[a] Department of Nuclear Physics, China Institute of Atomic Energy, Beijing, 102413, People's Republic of China
[b] Guangxi Key Laboratory of Nuclear Physics and Nuclear Technology, Guangxi Normal University, Guilin, 541004, People's Republic of China
[c] Key Laboratory of High Precision Nuclear Spectroscopy, Institute of Modern Physics, Chinese Academy of Sciences, Lanzhou 730000, People's Republic of China
[d] School of Nuclear Science and Technology, University of Chinese Academy of Sciences, Beijing, 100049, People's Republic of China
[e] Beijing Radiation Center, Beijing, 100875, People's Republic of China
[f] Key Laboratory of Beam Technology of Ministry of Education, College of Nuclear Science and Technology, Beijing Normal University, Beijing, 100875, People's Republic of China
[g] Center of Theoretical Nuclear Physics, National Laboratory of Heavy Ion Accelerator of Lanzhou, Lanzhou, 730000, People's Republic of China
[h] Department of Physics, Guangxi Normal University, Guilin, 541004, People's Republic of China

ARTICLE INFO

Article history:
Received 23 October 2020
Received in revised form 7 January 2021
Accepted 20 January 2021
Available online 8 February 2021
Editor: J.-P. Blaizot

ABSTRACT

The production cross sections for primary and residual fragments produced in two reaction systems ^{136}Xe + ^{198}Pt and ^{238}U + ^{198}Pt at incident energy 8 MeV/nucleon are calculated by improved quantum molecular dynamics (ImQMD) model incorporated with the statistical evaporation model (HIVAP code). It is found that the cross sections for n-rich $N = 126$ residual fragments are several times larger in ^{238}U+^{198}Pt than in ^{136}Xe+^{198}Pt due to the larger cross sections and lower excitation energies of primary fragments in ^{238}U induced reactions. In both systems, $N = 126$ semi-magic residues are produced via neutron emission in the decay of primary fragments, which survive in the semi-central collisions and have lower excitation energies.

The properties of n-rich $N = 126$ waiting point nuclei have the largest impact on the astrophysical *r*-process abundance peak around $A = 195$ and are extremely important for understanding the astrophysical nucleosynthesis [1]. The isotopes with extreme neutron-to-proton ratios in this region can be produced neither in fission nor in fusion reactions. Initially cold fragmentation of ^{208}Pb was used for the production of n-rich $N \sim 126$ nuclei below Pb by abrasion of protons from the projectile [2,3]. In recent ten years further progress was made by using the projectile fragmentation of ^{238}U beam, tens of heavy neutron-rich nuclei in the atomic number range of $60 \leq Z \leq 87$ were identified [4,5].

Multinucleon transfer (MNT) reactions with ^{208}Pb target at near-barrier energies were first proposed by Zagrebaev and Greiner to produce the n-rich $N = 126$ nuclei [6–8]. Calculations based on multi-dimensional Langevin equations indicated that tens of new nuclides could be produced in such reactions. Experimental studies of ^{136}Xe + ^{208}Pb reactions were performed at Dubna and Argonne to investigate the stabilizing effects of the neutron closed shells at $N = 82$ for ^{136}Xe and $N = 126$ for ^{208}Pb [9,10]. The ground state *Q*-value (Q_{gg}) favors the transfer of protons from lead to xenon, favorable for the production of $N \sim 126$ isotopes below ^{208}Pb. Calculations with the Grazing code suggested that the use of ^{198}Pt target may have significant advantage over ^{208}Pb because of larger transfer probability of neutron compared to proton [11]. The experimental measurement of products in ^{136}Xe + ^{198}Pt at $\sim$ 8 MeV/nucleon were carried out at GANIL [12]. The cross sections indirectly deduced for $N = 126$ isotones in ^{136}Xe + ^{198}Pt showed huge advantage of MNT reaction over the fragmentation of ^{208}Pb beam on Be target in the production of very neutron-rich nuclei with proton number $Z \leq 77$.

The advantage of the MNT reactions, such as ^{136}Xe + ^{198}Pt, ^{208}Pb, in the production of neutron-rich nuclei stimulated further theoretical studies using different models. The influence of shell effects and dynamical deformation on the potential energy surface and the mass distribution were investigated by the dinuclear system (DNS) model [13–15]. The angular distributions of neutron-rich nuclei with $N = 126$ were found to be strongly sensitive to the reaction dynamics and the collision energy in the Langevin-type approach [16]. By using improved quantum molecular dynam-

* Corresponding authors.
E-mail addresses: zhaokai@ciae.ac.cn (K. Zhao), liuzhong@impcas.ac.cn (Z. Liu).

https://doi.org/10.1016/j.physletb.2021.136101

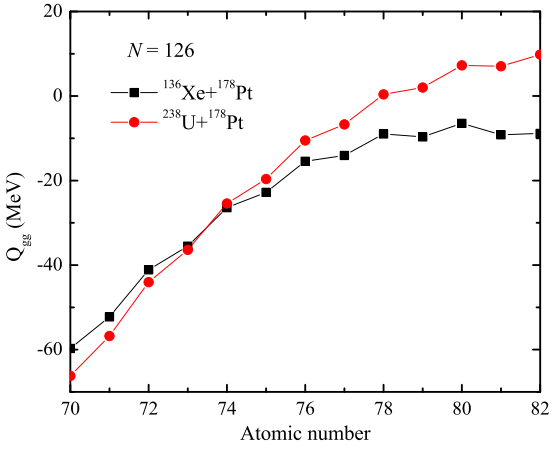

Fig. 1. Q-value of producing fragments with neutron number $N = 126$ in reactions of ^{136}Xe+^{198}Pt and ^{238}U+^{198}Pt. The unmeasured mass of nuclei are calculated from Ref. [24].

ics (ImQMD) model, the energy dissipation of the system ^{136}Xe + ^{198}Pt were found strongly associated with the incident energy [17]. Employing the quantal diffusion mechanism for multinucleon transfer in ^{136}Xe+^{208}Pb, the mass distribution of primary fragments and the production of several isotopes heavier than target were well reproduced by the stochastic mean-field (SMF) approach [18,19]. The time-dependent Hartree-Fock (TDHF) method with a statistical compound-nucleus deexcitation model (GEMINI++) provided good description of the yields of nuclei near the target. There still remained significant discrepancies between TDHF+GEMINI results and the measured cross sections when going away from the target nucleus [20,21]. So theoretical descriptions of multinucleon transfer processes beyond the standard self-consistent mean-field theory are necessary.

Considering a larger neutron excess in ^{238}U, the reaction system of ^{198}Pt + ^{238}U was proposed for the production of $N \sim 126$ n-rich nuclei by Zagrebaev and Greiner [8]. The calculated cross sections for new neutron-rich heavy nuclei in this reaction system at incident energy slightly below Bass barrier [22] are on average higher than those in the collision of ^{136}Xe or ^{192}Os with a ^{208}Pb target [8]. The calculated cross sections for neutron-rich isotopes around $N = 126$ by DNS model also showed advantage of using ^{238}U [23]. In terms of the ground state Q-values, ^{238}U has advantage over ^{136}Xe in reactions with ^{198}Pt target for producing primary fragments with neutron number $N = 126$ and proton number $Z \geq 74$, as shown in Fig. 1. The unmeasured mass of nuclei are calculated from Ref. [24]. For primary fragments with $Z < 74$, the Q_{gg} values are a little bit lower with ^{238}U than ^{136}Xe.

As the probabilities of multinucleon transfer between two colliding nuclei are energy sensitive, reactions at incident energies above Bass barrier need to be studied further. The processes of multinucleon transfer and production of primary fragments are closely related to a variety of degrees of freedom, such as deformations of two colliding nuclei, different types of separation of the composite system and the emission of light particles, etc. It is necessary to apply a microscopic transport model to simulate the whole dynamical process from the touching of projectile and target to the production of primary fragments. In this paper, the improved quantum molecular dynamics (ImQMD) model is used to simulate the reactions of ^{136}Xe, ^{238}U + ^{198}Pt at incident energy 8 MeV/nucleon. The cross sections for primary fragments with $N = 126$ in the two systems are calculated and compared. By incorporating the statistical evaporation model (HIVAP code), we further analyze the production mechanism of the residual fragments with $N = 126$. The beam energy of 8 MeV/nucleon is chosen for the comparison with the experimental results [12].

Table 1
The model parameters.

α (MeV)	β (MeV)	γ	g_0 (MeV fm^2)	
−356	303	7/6	7.0	
g_τ (MeV)	η	c_s (MeV)	κ_s (fm^2)	ρ_0 (fm^{-3})
12.5	2/3	32	0.08	0.165

In ImQMD model, each nucleon is represented by a coherent state of a Gaussian wave packet. The time evolution of the coordinate and momentum of each nucleon in the mean-field part is determined by Hamiltonian equations. The Hamiltonian includes kinetic energy, nuclear potential energy and the Coulomb energy. The nuclear potential energy is an integration of the Skyrme type potential energy density functional, which reads

$$V_{\rm loc} = \frac{\alpha}{2}\frac{\rho^2}{\rho_0} + \frac{\beta}{\gamma+1}\frac{\rho^{\gamma+1}}{\rho_0^{\gamma}} + \frac{g_0}{2\rho_0}(\nabla\rho)^2 + \frac{c_s}{2\rho_0}[\rho^2 - \kappa_s(\nabla\rho)^2]\delta^2 + g_\tau\frac{\rho^{\eta+1}}{\rho_0^{\eta}}, \quad (1)$$

where $\rho = \rho_n + \rho_p$ is the nucleon density and $\delta = (\rho_n - \rho_p)/(\rho_n + \rho_p)$. ρ_n, ρ_p are neutron and proton density, respectively. The Coulomb energy in the Hamiltonian is written as a sum of the direct and the exchange contribution:

$$U_{\rm Coul} = \frac{1}{2}\int\int \rho_p(\mathbf{r})\frac{e^2}{|\mathbf{r}-\mathbf{r}'|}\rho_p(\mathbf{r}')d\mathbf{r}d\mathbf{r}' - e^2\frac{3}{4}\left(\frac{3}{\pi}\right)^{1/3}\int \rho_p^{4/3}d\mathbf{r}. \quad (2)$$

In nucleon-nucleon collision part, the isospin-dependent in-medium nucleon-nucleon scattering cross sections are applied, and the Pauli blocking effects are treated as in Ref. [25]. The phase space occupation number constraint method [26] is adopted in this model. The model parameters as those used in Ref. [27] are listed in Table 1. More detailed description of the ImQMD model and its applications can be found in Refs. [28–30].

In this work, the binding energy per nucleon and deformation of ^{136}Xe, ^{238}U and ^{198}Pt are taken from Ref. [31]. The initial orientations of the projectile and target in all events are sampled randomly with an equal probability. The cross section for the primary fragment with charge number Z, mass number A, excitation energy E^* is calculated by

$$\sigma(Z, A, E^*, J) = \sum_{b=0}^{b_{\rm max}} 2\pi b\Delta b\frac{N_{\rm frag}(Z, A, b, E^*, J)}{N_{\rm tot}(b)}. \quad (3)$$

Here b is the impact parameter, $N_{\rm frag}(Z, A, b, E^*, J)$ is the number of events in which a fragment (Z, A, E^*, J) is formed at a given impact parameter b. The excitation energy E^* for the fragment with charge number Z and mass number A is obtained by subtracting the corresponding ground-state energy [31] from the total energy of the excited fragment in its rest frame. Angular momentum J of primary fragment is calculated by the coordinates and momentums of all nucleons in the rest frame of fragment. $N_{\rm tot}(b)$ is the total event number at a given impact parameter b. The maximum impact parameter is taken to be $b_{\rm max} = 1.2(A_P^{1/3}+A_T^{1/3})$ fm, where A_P and A_T are the mass number of projectile and target respectively. The impact parameter step is $\Delta b = 0.1$ fm. The initial distance between the centers of mass of projectile and target is taken to be 30 fm. 10,000 events for each impact parameter are simulated in this work.

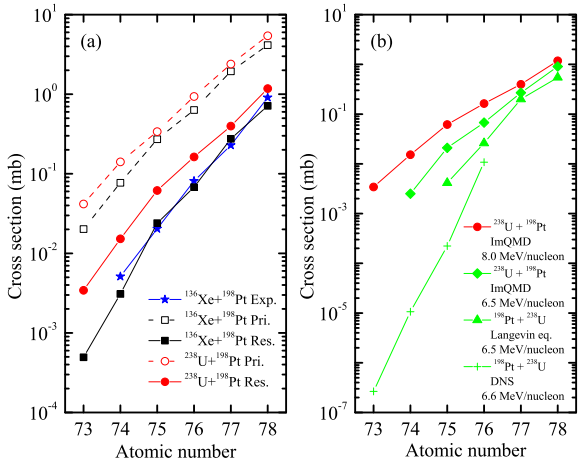

Fig. 2. Cross sections for $N = 126$ isotones as a function of atomic number. In panel (a), the squares and circles represent the calculation results in ^{136}Xe+^{198}Pt and ^{238}U+^{198}Pt at 8 MeV/nucleon. The stars are from the experimentally deduced results of ^{136}Xe+^{198}Pt at ∼8 MeV/nucleon in Ref. [12]. Open and solid shapes denote primary and residual fragments, respectively. For the reactions of ^{238}U with ^{198}Pt at ∼6.5 MeV/nucleon in panel (b), the results of ImQMD model, Langevin-type equations and DNS model are compared with diamond, triangles and crosses respectively. The calculation results of Langevin-type equations and DNS model are taken from Ref. [8] and Ref. [23].

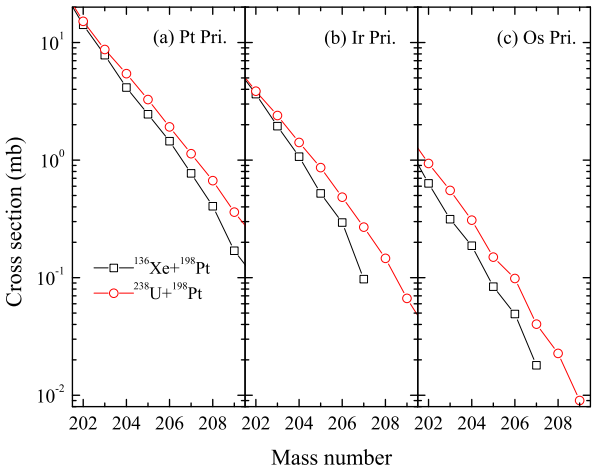

Fig. 3. Cross sections for primary fragment with neutron number $N \geq 126$. The meaning of symbols is the same as Fig. 2.

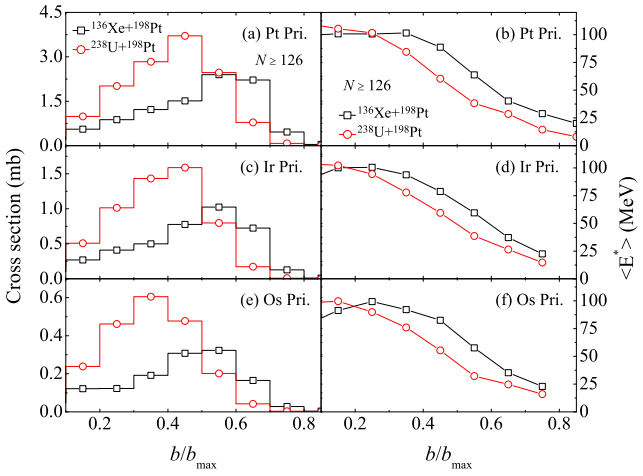

Fig. 4. Cross sections (left panels) and average excitation energies (right panels) of primary fragments with $N \geq 126$ of three elements Os, Ir and Pt as a function of impact parameters. The meaning of symbols is the same as Fig. 2.

At 1000 fm/c after the re-separation of the composite system, ImQMD simulation is terminated and primary fragments are recognized at this time as done in Ref. [32]. The de-excitation process, including the evaporation of γ, neutron, proton, α particle and fission, for each excited primary fragment is performed by using the statistical evaporation model (HIVAP code) [33,34].

The calculated cross sections for $N = 126$ primary and residual isotones of $Z \leq 78$ produced in ^{136}Xe, ^{238}U+^{198}Pt at incident energy 8 MeV/nucleon are shown in Fig. 2 (a). The results of the two reaction systems are represented by squares and circles, respectively. Primary and residual fragments are denoted by open and solid symbols, respectively. Stars are experimental data for the ^{136}Xe+^{198}Pt reaction at ∼8 MeV/nucleon deduced in Ref. [12]. The calculated cross sections for primary and residual fragments along $N = 126$ decrease approximately exponentially with decreasing atomic number. For primary fragments produced in ^{238}U+^{198}Pt, the cross sections are generally larger than those in ^{136}Xe+^{198}Pt. Compared with primary fragments, the cross sections for residues decrease by about one order of magnitude in both systems. The calculated cross sections for residual $N = 126$ isotones in ^{136}Xe+^{198}Pt reaction are in good agreement with the experimentally deduced results. The cross sections for $N = 126$ residues in ^{238}U+^{198}Pt are higher than those in ^{136}Xe+^{198}Pt. Their difference increases with decreasing atomic number, up to a factor of about seven at $Z = 73$. To investigate the influence of incident energy on the production of $N = 126$ neutron-rich nuclei in ^{238}U+^{198}Pt, the cross sections for these residual nuclei are calculated by ImQMD model at 6.5 MeV/nucleon (around Bass barrier) and presented with diamond symbols in Fig. 2 (b). It shows that the incident energies above the barrier provide several times higher cross sections for these neutron-rich nuclei. The cross sections calculated by Langevin-type equations [8] and DNS [23] for the reactions of ^{198}Pt with ^{238}U at ∼6.5 MeV/nucleon are also shown in panel (b) for comparison. The difference between the results of three methods increases gradually with the decrease of atomic number. The cross sections for the neutron-rich nuclei by Langevin-type equations are smaller than those of ImQMD and the difference is within one magnitude. But The results of DNS are smaller by several orders of magnitude than those of ImQMD and Langevin-type equations, especially for neutron-rich nuclei with smaller atomic number.

In the following, we focus on the difference between ^{136}Xe+^{198}Pt and ^{238}U+^{198}Pt at 8 MeV/nucleon for the production mechanisms of $N = 126$ neutron-rich nuclei. Fig. 3 shows the calculated cross sections for primary isotopes of Pt, Ir and Os with neutron number $N \geq 126$. For each isotopic chain, the cross sections decrease roughly exponentially and the difference between these two systems increases gradually with increasing mass number. It indicates that the ^{238}U induced reactions are more favorable for the production of heavier n-rich nuclei.

The variation of the cross sections and excitation energies of the $N \geq 126$ primary fragments of Pt, Ir and Os with the impact parameter are shown in Fig. 4. In both reaction systems, the cross sections for these primary fragments peak around the reduced impact parameters corresponding to semi-central collisions, at a smaller value of $b/b_{max} = 0.3$–0.5 for the ^{238}U+^{198}Pt reaction, while for ^{136}Xe+^{198}Pt, $b/b_{max} = 0.5$–0.6. The difference originates mainly from the different ratios between the incident energy and the reaction barrier for the two reactions. The incident energy 8 MeV/nucleon corresponds to $1.2V_B$ for ^{238}U+^{198}Pt and $1.5V_B$ for ^{136}Xe+^{198}Pt, where V_B is Bass barrier [22]. At smaller relative incident energy, the multinucleon transfer mainly occurs at lower impact parameters because relative collective kinetic energy between projectile and target is needed to penetrate the barrier. The influence of different relative incident energies between

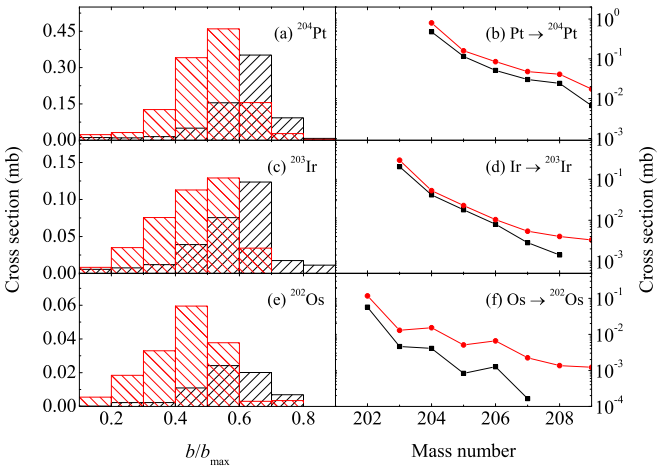

Fig. 5. Left panels: Cross sections for residual fragments ^{202}Os, ^{203}Ir and ^{204}Pt as a function of impact parameters. Right panels: The contributions to the cross sections of residual fragments ^{202}Os, ^{203}Ir and ^{204}Pt from the primary fragments of three elements.

two systems on the average excitation energies $< E^* >(Z,b) = [\sum_A E^*\sigma(Z,A,E^*,b)]/[\sum_A \sigma(Z,A,E^*,b)]$ of the same primary fragments is also shown in the right panels of Fig. 4. The average excitation energies in ^{238}U+^{198}Pt are generally smaller than those in ^{136}Xe+^{198}Pt, especially for the semi-central collisions. In ^{238}U+^{198}Pt, the incident energy is smaller relative to the barrier, the cross sections are generally larger than those in ^{136}Xe+^{198}Pt, mainly due to the larger neutron excess in ^{238}U than ^{136}Xe.

The productions of residual fragments ^{204}Pt, ^{203}Ir and ^{202}Os are shown in Fig. 5. In the left panels, the cross sections for these $N = 126$ residues produced in ^{238}U+^{198}Pt are generally larger than in ^{136}Xe+^{198}Pt, especially for lower impact parameters. Most of them are produced in the semi-central collisions with reduced impact parameters $b/b_{max} = 0.4$–0.7. Compared with the cross sections for primary fragments in Fig. 4, a shift of the peak cross section to larger reduced impact parameters can be seen. Most of the primary fragments are produced with lower excitation energies in collisions at $b/b_{max} = 0.3$–0.6. The contributions of the $N \geq 126$ primary fragments of Pt, Ir and Os to the productions of their respective $N = 126$ residues ^{204}Pt, ^{203}Ir and ^{202}Os are shown in right panels of Fig. 5. Over 99% of these $N = 126$ isotones are produced in the decay of primary fragments of the same element via neutron emission. The contributions to the cross sections for their $N = 126$ isotones decrease with the mass number of fragments. The highest portion are from primary fragments of ^{204}Pt, ^{203}Ir and ^{202}Os at lower excitation energies respectively.

Multi-nucleon transfer reactions ^{136}Xe, ^{238}U + ^{198}Pt at incident energy 8 MeV/nucleon are simulated by improved quantum molecular dynamics model incorporated with the statistical evaporation model (HIVAP code). The use of ^{238}U shows an obvious advantage in producing more neutron-rich primary and residual fragments over ^{136}Xe. The reaction system ^{238}U+^{198}Pt has larger neutron-to-proton ratio and larger Q-value for producing fragments of $Z \geq 74$ with $N = 126$. At lower relative incident energy to the barrier, it provides larger cross sections for primary fragments with neutron number $N \geq 126$ and smaller excitation energies. The enhanced production of primary fragments with neutron number $N = 126$ in ^{238}U + ^{198}Pt should be related to the effect of Q-value, isospin diffusion and the fluctuation of multi-nucleon transfer, etc. Although the Q-value is almost the same for the fragments of the $N = 126$ residues with $Z = 73,74$ in the two systems, the cross sections is still significantly larger in ^{238}U + ^{198}Pt than ^{136}Xe + ^{198}Pt. It shows the important roles of neutron excess in two colliding nuclei and the dynamical effect in multi-nucleon transfer in the production of neutron-rich exotic nuclei. The dependence of incident energy on the production of $N = 126$ neutron-rich nuclei are found in the reaction of ^{238}U + ^{198}Pt in the comparison between the results of near (6.5 MeV/nuclon) and above (8 MeV/nucleon) Bass barrier. It shows the advantage for producing $N = 126$ neutron-rich nuclei above (8 MeV/nucleon) Bass barrier. Near Bass barrier, the calculated cross sections for $N = 126$ neutron-rich nuclei by using ImQMD model and Langevin-type equations are closer. Both are several orders of magnitude larger than those in DNS model, especially for the nuclei of $Z = 73,74$. The mechanisms of multinucleon transfer in ^{238}U + ^{198}Pt is found to be more complicated than ^{136}Xe + ^{198}Pt. And more details can be revealed by further investigations.

Kai Zhao is grateful to X.D. Tang and Z.G. Gan for insightful discussion about the multinucleon transfer reactions. This work is supported by National Natural Science Foundation of China under Grant No. 11675266, 11635003, 11161130520, 11965004, 11961141004, 11735017, 11675225, U1867212, the Continuous Basic Scientific Research Project No. WDJC-2019-13, the Leading Innovation Project under Grant No. LC192209000701, LC202309000201, the Open Project of Guangxi Key Laboratory of Nuclear Physics and Nuclear Technology No. NLK2020-01, the National Key R&D Program of China (Contract No. 2018YFA0404402), and the Strategic Priority Research Program of Chinese Academy of Sciences, Grant No. XDB34000000. The Project was Funded by the Key Laboratory of High Precision Nuclear Spectroscopy, Institute of Modern Physics, Chinese Academy of Sciences. We also acknowledge support by the Supercomputer Center of HIRFL at Institute of Modern Physics.

Declaration of competing interest

The authors declare that they have no known competing financial interests or personal relationships that could have appeared to influence the work reported in this paper.

References

[1] F. Käppeler, F.-K. Thielemann, M. Wiescher, Annu. Rev. Nucl. Part. Sci. 48 (1998) 175.
[2] T. Kurtukian-Nieto, J. Benlliure, K.-H. Schmidt, L. Audouin, F. Becker, B. Blank, I.N. Borzov, E. Casarejos, M. Fernández-Ordóñez, J. Giovinazzo, D. Henzlova, B. Jurado, K. Langanke, G. Martínez-Pinedo, J. Pereira, F. Rejmund, O. Yordanov, Nucl. Phys. A 827 (2009) 587c.
[3] T. Kurtukian-Nieto, J. Benlliure, K.-H. Schmidt, L. Audouin, F. Becker, B. Blank, E. Casarejos, F. Farget, M. Fernández-Ordóñez, J. Giovinazzo, D. Henzlova, B. Jurado, J. Pereira, O. Yordanov, Phys. Rev. C 89 (2014) 024616.
[4] H. Alvarez-Pol, J. Benlliure, E. Casarejos, L. Audouin, D. Cortina-Gil, T. Enqvist, B. Fernández-Domínguez, A.R. Junghans, B. Jurado, P. Napolitani, J. Pereira, F. Rejmund, K.-H. Schmidt, O. Yordanov, Phys. Rev. C 82 (2010) 041602(R).
[5] J. Kurcewicz, F. Farinon, H. Geissel, S. Pietri, C. Nociforo, A. Prochazka, H. Weick, J.S. Winfield, A. Estradé, P.R.P. Allegro, A. Bail, G. Béier, J. Benlliure, G. Benzoni, M. Bunce, M. Bowry, R. Caballero-Folch, I. Dillmann, A. Evdokimov, J. Gerl, A. Gottardo, E. Gregor, R. Janik, A. Kelić-Heil, R. Knöbel, T. Kubo, Yu.A. Litvinov, E. Merchan, I. Mukha, F. Naqvi, M. Pfützner, M. Pomorski, Zs. Podolyák, P.H. Regan, B. Riese, M.V. Ricciardi, C. Scheidenberger, B. Sitar, P. Spiller, J. Stadlmann, P. Strmen, B. Sun, I. Szarka, J. Taïeb, S. Terashima, J.J. Valiente-Dobón, M. Winkler, Ph. Woods, Phys. Lett. B 717 (2012) 371.
[6] V. Zagrebaev, W. Greiner, J. Phys. G, Nucl. Part. Phys. 35 (2008) 125103.
[7] V. Zagrebaev, W. Greiner, Nucl. Phys. A 834 (2010) 366c.
[8] V. Zagrebaev, W. Greiner, Phys. Rev. C 87 (2013) 034608.
[9] E.M. Kozulin, E. Vardaci, G.N. Knyazheva, A.A. Bogachev, S.N. Dmitriev, I.M. Itkis, M.G. Itkis, A.G. Knyazev, T.A. Loktev, K.V. Novikov, E.A. Razinkov, O.V. Rudakov, S.V. Smirnov, W. Trzaska, V.I. Zagrebaev, Phys. Rev. C 86 (2012) 044611.
[10] J.S. Barrett, W. Loveland, R. Yanez, S. Zhu, A.D. Ayangeakaa, M.P. Carpenter, J.P. Greene, R.V.F. Janssens, T. Lauritsen, E.A. McCutchan, A.A. Sonzogni, C.J. Chiara, J.L. Harker, W.B. Walters, Phys. Rev. C 91 (2015) 064615.
[11] R. Yanez, W. Loveland, Phys. Rev. C 91 (2015) 044608.
[12] Y.X. Watanabe, Y.H. Kim, S.C. Jeong, Y. Hirayama, N. Imai, H. Ishiyama, H.S. Jung, H. Miyatake, S. Choi, J.S. Song, E. Clement, G. de France, A. Navin, M. Rejmund, C. Schmitt, G. Pollarolo, L. Corradi, E. Fioretto, D. Montanari, M. Niikura, D. Suzuki, H. Nishibata, J. Takatsu, Phys. Rev. Lett. 115 (2015) 172503.

[13] Z.Q. Feng, Phys. Rev. C 95 (2017) 024615.
[14] L. Zhu, P.W. Wen, C.J. Lin, X.J. Bao, J. Su, C. Li, C.C. Guo, Phys. Rev. C 97 (2018) 044614.
[15] S.Q. Guo, X.J. Bao, H.F. Zhang, J.Q. Li, Nan Wang, Phys. Rev. C 100 (2019) 054616.
[16] A.V. Karpov, V.V. Saiko, Phys. Rev. C 96 (2017) 024618.
[17] C. Li, X.X. Xu, J.J. Li, G. Zhang, B. Li, C.A.T. Sokhna, Z.S. Ge, F. Zhang, P.W. Wen, F.S. Zhang, Phys. Rev. C 99 (2019) 024602.
[18] S. Ayik, B. Yilmaz, O. Yilmaz, A.S. Umar, Phys. Rev. C 100 (2019) 014609.
[19] S. Ayik, O. Yilmaz, B. Yilmaz, A.S. Umar, Phys. Rev. C 100 (2019) 044614.
[20] K. Sekizawa, Phys. Rev. C 96 (2017) 014615.
[21] X. Jiang, N. Wang, Phys. Rev. C 101 (2020) 014604.
[22] R. Bass, Nuclear Reactions with Heavy Ions, Springer-Verlag, Berlin, 1980.
[23] L. Zhu, C. Li, J. Su, C.C. Guo, W. Hua, Phys. Lett. B 791 (2019) 20.
[24] N. Wang, M. Liu, X.Z. Wu, J. Meng, Phys. Lett. B 734 (2014) 215.
[25] Q.F. Li, Z.X. Li, Phys. Rev. C 64 (2001) 064612.
[26] M. Papa, T. Maruyama, Aldo Bonasera, Phys. Rev. C 64 (2001) 024612.
[27] K. Zhao, Z.X. Li, Y.X. Zhang, N. Wang, Q.F. Li, C.W. Shen, Y.J. Wang, X.Z. Wu, Phys. Rev. C 94 (2016) 024601.
[28] N. Wang, Z.X. Li, X.Z. Wu, Phys. Rev. C 65 (2002) 064608.
[29] N. Wang, Z.X. Li, X.Z. Wu, J.L. Tian, Y.X. Zhang, M. Liu, Phys. Rev. C 69 (2004) 034608.
[30] N. Wang, Z.X. Li, X.Z. Wu, E.G. Zhao, Mod. Phys. Lett. A 20 (2005) 2619.
[31] P. Möller, J.R. Nix, W.D. Myers, W.J. Swiatecki, At. Data Nucl. Data Tables 59 (1995) 185.
[32] K. Zhao, Z.X. Li, N. Wang, Y.X. Zhang, Q.F. Li, Y.J. Wang, X.Z. Wu, Phys. Rev. C 92 (2015) 024613.
[33] C.W. Shen, G. Kosenko, Y. Abe, Phys. Rev. C 66 (2002) 061602(R).
[34] W. Reisdorf, F.P. Hessberger, K.D. Hildenbrand, S. Hofmann, G. Münzenberg, K.-H. Schmidt, W.F.W. Schneider, K. Sümmerer, G. Wirth, J.V. Kratz, K. Schutt, C.-C. Sahm, Nucl. Phys. A 444 (1985) 154.